Dual phase grating interferometer for tunable dark-field sensitivity

Kagias, Matias ; Wang, Zhentian ; Jefimovs, Konstantins ; Stampanoni, Marco

Abstract: Hard X-ray dark-field and phase contrast imaging using grating interferometry have shown great potential for medical and industrial applications. However, the wide spread applicability of the method is challenged by a number of technical related issues such as relatively low dose and flux efficiency due to the absorption grating, fabrication of high quality absorption gratings, slow data acquisition protocol and high mechanical stability requirements. In this paper, the authors propose an interferometric method for dark-field and differential phase contrast imaging based on phase shifting elements only with the purpose to improve the dose and flux efficiency and simplify the setup. The proposed interferometer consists of two identical phase gratings of small pitch (1.3 m), which generate an interference fringe at the detector plane with a large enough pitch that can be resolved directly. In particular, the system exhibits flexible and tunable dark-field sensitivity which is advantageous to probe unresolvable micro-structure in the sample. Experiments on a micro focal tube validated the method and demonstrated the versatility and tunability of the system compared to conventional Talbot grating interferometer.

DOI: https://doi.org/10.1063/1.4973520

Dual phase grating interferometer for tunable dark-field sensitivity

Matias Kagias, Zhentian Wang, Konstantins Jefimovs, and Marco Stampanoni

Citation: Appl. Phys. Lett. **110**, 014105 (2017); doi: 10.1063/1.4973520
View online: https://doi.org/10.1063/1.4973520
View Table of Contents: http://aip.scitation.org/toc/apl/110/1
Published by the American Institute of Physics

Dual phase grating interferometer for tunable dark-field sensitivity

Matias Kagias,[1,2] Zhentian Wang,[1,2,a)] Konstantins Jefimovs,[1,2] and Marco Stampanoni[1,2]
[1]*Swiss Light Source, Paul Scherrer Institute, 5232 Villigen, Switzerland*
[2]*Institute for Biomedical Engineering, University and ETH Zurich, 8092 Zurich, Switzerland*

(Received 10 November 2016; accepted 16 December 2016; published online 4 January 2017)

Hard X-ray dark-field and phase contrast imaging using grating interferometry have shown great potential for medical and industrial applications. However, the wide spread applicability of the method is challenged by a number of technical related issues such as relatively low dose and flux efficiency due to the absorption grating, fabrication of high quality absorption gratings, slow data acquisition protocol and high mechanical stability requirements. In this paper, the authors propose an interferometric method for dark-field and differential phase contrast imaging based on phase shifting elements only with the purpose to improve the dose and flux efficiency and simplify the setup. The proposed interferometer consists of two identical phase gratings of small pitch (1.3 μm), which generate an interference fringe at the detector plane with a large enough pitch that can be resolved directly. In particular, the system exhibits flexible and tunable dark-field sensitivity which is advantageous to probe unresolvable micro-structure in the sample. Experiments on a micro focal tube validated the method and demonstrated the versatility and tunability of the system compared to conventional Talbot grating interferometer. *Published by AIP Publishing.*
[http://dx.doi.org/10.1063/1.4973520]

Talbot(-Lau) grating interferometry (GI)[1–3] is a phase sensitive imaging method that has great potential for a number of medical and industrial applications.[4–12] GI provides access to three complementary signals simultaneously: the conventional absorption, the differential phase contrast (DPC) related to refraction of the incoming beam and the visibility reduction that relates to the small angle scattering (SAXS) taking place in the sample and is well known under the term dark-field.[13] Both differential phase and dark-field can provide additional information about the sample to the conventional absorption contrast. Specifically, the DPC signal is highly sensitive to fine electron density variations in the sample, which results in a higher contrast for soft tissues or low-Z materials. The dark-field signal can reveal structural information about the unresolved microstructure of the sample in a size scale beyond the resolution capabilities of the detecting system.[15,16] The usual realisation of a GI is the Talbot-Lau interferometer consisting of three gratings G_0, G_1 and G_2.[17] The first grating G_0 (absorption grating) is optionally used to generate enough spatial coherence when X-ray sources with a large focal size are used. G_1 is a phase grating that splits the beam and generates an interference pattern at the Talbot distances, and G_2 (absorption grating) is used to sample the generated interference fringe. This is done by a procedure called phase stepping, where G_2 is usually scanned for one or more periods of the interference fringe and images are acquired at each step. This configuration allows to decouple the detector resolution from the grating pitch but relies on the fabrication of high aspect ratio metal structures (G_2)[14,18] and further reduces the flux and dose efficiency, which is crucial for medical applications due to the additional photon loss after the sample. Therefore, a technique based only on phase shifting elements is favourable.[19,20] Moreover, for the investigation of unresolved microstructures by means of the dark-field signal multiple measurements at different correlation lengths need to be performed.[15,16,21] The correlation length ξ basically depends on three factors: wavelength λ, sample to detector distance L_s, and the period of the interference fringe p. The proposed methods so far focus on moving the sample between the detector and the phase grating G_1 in order to scan at different correlation lengths.[21,22] Nonetheless, such an approach has a number of limitations. Primarily, when a cone beam geometry is considered, the sample magnification changes, meaning that additional computation steps, such as image registration, are required for analysing the data. Additionally, this might not be feasible depending on the length of the interferometer compared to the analysed sample. A different approach makes use of the change of the wavelength λ;[23] however, implementing such an approach on an X-ray tube setup would require spectral detectors that still are not widely available. In order to tackle all these limitations, an interferometer that can change its correlation length in a robust way without major geometrical changes would be beneficial.

In this work, we examine the possibility of combining two phase gratings to perform absorption, differential phase contrast, and tunable dark-field imaging. Such configurations, operated in parallel beam geometry, have been shown to produce fringes for a wide range of distances in the visible light regime.[24] Our implementation is based on two identical silicon phase gratings of a period of 1.3 μm covering an area of $5.5 \times 7.5\,\mathrm{cm}^2$. Specifically, by varying the distance between the two phase gratings, the fringe period can be modulated that allows to tune the length scale sensitivity[21] of the system and perform scans that can provide additional insight into the sample microstructure.

A schematic of a generic implementation of the proposed interferometer is shown in Figure 1. The principle and design of the setup can be imagined as a conjunction of two

a)zhentian.wang@psi.ch

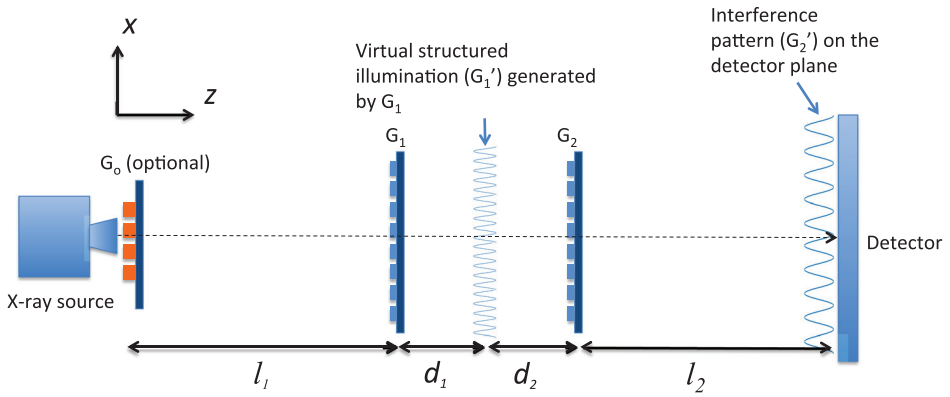

FIG. 1. Sketch of the proposed dual phase grating interferometer. An absorption grating G_0 is optionally used to increase the coherence of the X-ray source if necessary. The first phase grating G_1 is placed at distance l_1 from the X-ray source. The second grating G_2 is placed at distance $d_1 + d_2$ from G_1 and the X-ray detector is placed at distance l_2 from G_2.

conventional Talbot-Lau grating interferometers. The first phase grating G_1 introduces a modulation to the phase of the incoming X-rays. Due to the Talbot effect, an intensity distribution will be generated at specific distances. This distribution will act as virtual structured illuminations onto the second phase grating G_2 to generate a large pitch fringe at the detector plane. The generated fringe at the detector plane should be large enough to be sampled without aliasing artefacts by the detector in use. Moreover, a total length of approximately 1.1 m is designed in order to have a relatively compact system. In the current implementation, we choose a symmetric design ($l_1 = l_2 = 1$ and $d_1 = d_2 = d$) with both gratings of 1.3 μm pitch for the sake of convenience. The gratings were etched to a depth of 23 μm that introduces a π phase shift at 17 keV. At this energy, the distances were defined to be $l = 50$ mm and $d = 5$ mm, and we will refer to these distances as nominal. It will be demonstrated that such an interferometer can still perform when deviating from its nominal imaging conditions without a considerable loss in performance due to its polychromatic character. The sample is placed right before the grating G_1 that results in an effective magnification of approximately two.

A microfocal X-ray tube was used as an X-ray source with a source size of 9.5 μm (70 kVp and 100 μA). The detection was performed with a Princeton Instruments PI-SCX:4300 X-ray detector. The pixel size of the detector was 24 μm allowing to record fringes with a period down to 100 μm. Taking into account the two-fold magnification, the effective imaging field of view (FOV) was $2.5 \times 2.5\,\text{cm}^2$. The PI-SCX:4300 X-ray detector is equipped with a Gd_2O_2S:Tb (Gadox) scintillator, which is very efficient at energies up to 20 keV (50% efficiency).

The system can be operated in two imaging protocols: single shot and phase stepping. In the single shot protocol, fast and straightforward imaging can be performed with trade off in image resolution. The retrieved image resolution is defined by the period of the generated fringe, which has to be larger than the detector resolution. In the case of phase stepping, one of the two gratings is shifted by one or more periods, which results in a shift of the observed interference fringe at the detector plane. An image is recorded for each phase step, allowing us to record a period of the interference fringe at each pixel. The resolution of the detector is maintained, however multiple exposures are necessary as well as appropriate motors to move one of the two gratings with sub-micrometer steps. The retrieval of the three complimentary signals is identical to the methods used in the standard grating interferometry when phase stepping is used[13] or based on the spatial Fourier transform in the case of single shot imaging.[25]

Before presenting a few imaging examples, we evaluated the system performance for different intergrating distances $d_1 + d_2$ in order to demonstrate the robustness of such a configuration. The evaluation was based on two metrics: fringe visibility and phase sensitivity. Both of them were calculated with the phase stepping approach. Under the assumption that one of the two gratings is scanned for one period, the visibility is given by

$$V^{i,j} = 2\frac{a_1^{i,j}}{a_0^{i,j}}, \tag{1}$$

where $a_1^{i,j}$ and $a_0^{i,j}$ are the first and zeroth harmonic of the phase stepping curve at pixel i,j. We calculated the mean visibility for different intergrating distances. The tube voltage

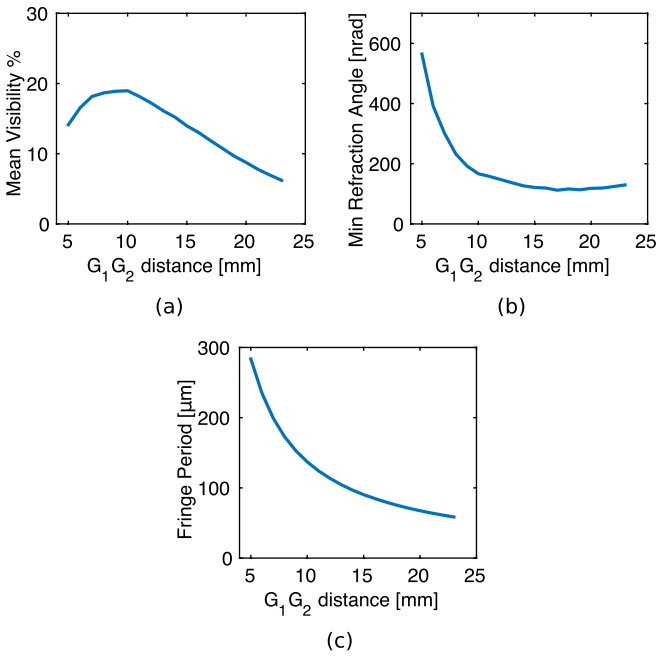

FIG. 2. Measured (a) visibility, (b) differential phase sensitivity, and (c) interference fringe period of dual phase grating interferometer for a total of 5 phase steps with 60 s exposure time and X-ray tube running at 70 kVp and 100 μA. The distance between the gratings was varied from 5 mm to 23 mm with steps of 1 mm. The visibility shows a clear maximum at around 10 mm, while the sensitivity seems to be constant for a large range of values demonstrating the versatility of the system.

was set to 70 kVp and the current to 100 μA.[26] A total of 5 phase steps over one period were acquired at each distance with an exposure time of 60 s each. In Figure 2(a), we can see how the mean visibility varies for the different distances. The maximum is obtained at an intergrating distance of approximately 10 mm (nominal distance). Although the fringe visibility is widely used for the characterisation of interferometric systems, the phase sensitivity can provide additional insight on the performance when acquiring DPC images. The phase sensitivity can be retrieved from the standard deviation σ_{DPC} of the background of a DPC image.[27] The σ_{DPC} is related to the minimum detectable refractive angle by

$$\alpha_{min} = p\frac{\sigma_{DPC}}{2\pi l_2}, \tag{2}$$

where p is the fringe pitch. We imaged a water phantom (Eppendorf tube) at different distances in order to retrieve the DPC signal and calculated the phase sensitivity, which is plotted in Figure 2(b). The curve shows that the phase sensitivity is more or less constant for a large range of values in comparison to the visibility measurement. This indicates that DPC imaging can be performed for a large range of intergrating distances.

The system can be used for conventional DPC imaging; however, in this paper, we focus on the length scale tunability of the system for dark-field imaging. The length scale sensitivity of an interferometer is characterised by the correlation length[16,21]

$$\xi = \frac{\lambda_{eff} L_s}{p}, \tag{3}$$

where λ_{eff} is the effective energy of the system that was found to be 22.8 keV, L_s is the sample to detector distance and p is the interference fringe pitch. For a fixed design of a Talbot-Lau interferometer, the only way of tuning the correlation length is by changing L_s. However, changing L_s will result in different magnifications for the sample in cone beam geometry, which complicates further data analysis and

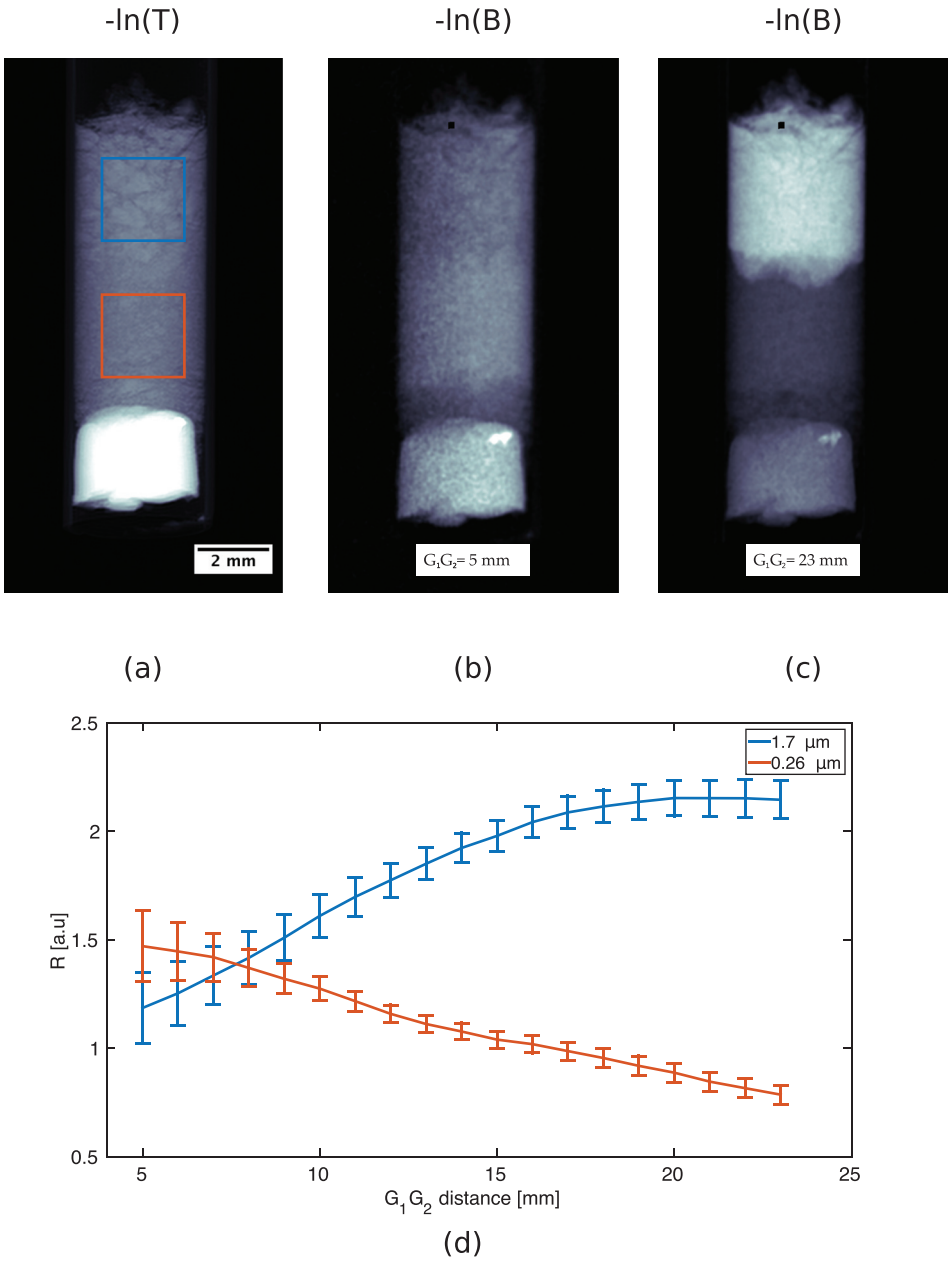

FIG. 3. (a) Absorption image of the two SiO_2 powders. Retrieved dark-field signal at (b) 5 mm and (c) 23 mm intergrating distance. (d) By tuning the intergrating distance, the R value changes for both powders showing the tunability of our system.

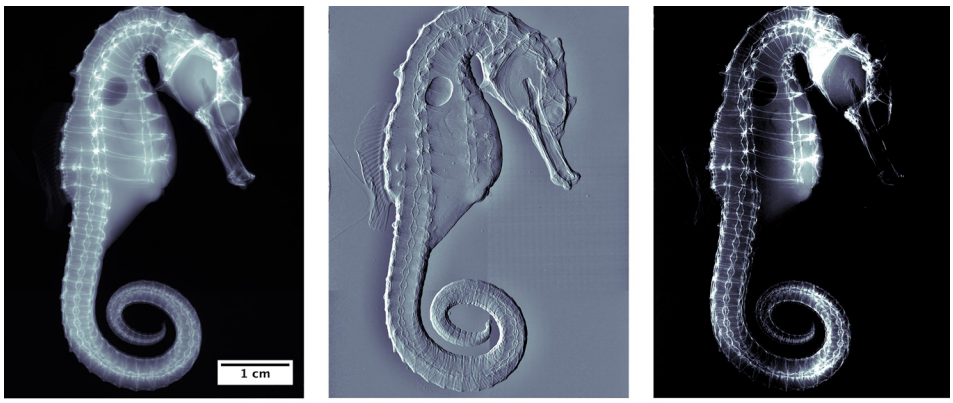

(a) (b) (c)

FIG. 4. (a) Absorption, (b) differential phase, and (c) dark-field images of a big belied seahorse.

sometimes might not even be possible. With the proposed system, ξ can be changed by tuning the intergrating distance by a few millimetres, which changes the fringe period p, as seen in Figure 2(c), and this does not affect the magnification of the system and in principle does not change its geometry neither. The change in length scale sensitivity was demonstrated by imaging a powder sample consisting of two SiO_2 powders produced by Cospheric LLC, USA,[28] of different mean grain sizes of 1.7 μm and 0.26 μm. The powders were placed in the same cylindrical container one on top of the other and imaged for intergrating distances ranging from 5 to 23 mm with a step of 1 mm. This resulted in a change in the correlation length from 103 nm to 458 nm approximately. The signals from the powders changed significantly, especially for the coarser powder the signal almost doubled. Another interesting observation was the contrast inversion between the two powders. To quantify the difference between the two powders, we calculated the thickness independent R value[9]

$$R = \frac{\ln B}{\ln T}, \tag{4}$$

where B is the visibility reduction and T is the transmission.[13] In Figure 3(d), the R values for the two different powders are plotted for each intergrating distance. The change in the strength of the dark-field signal for the two powders can clearly be seen from the two dark-field images at intergrating distances of 5 and 23 mm in Figures 3(b) and 3(c), respectively. For the sake of completeness, we also show the absorption image ($-\ln T$) in Figure 3(a) that stays constant for the different distances.

A big bellied seahorse was imaged in the single shot mode to demonstrate the imaging capability of the system for biomedical applications. The sample was imaged with the same conditions as the characterisation tests. In order to image the complete sample, stitching was performed using $2\,\mathrm{H} \times 3\,\mathrm{V}$ FOVs with an appropriate overlap to allow lossless stitching. The resulting images after stitching are shown in Figure 4.

To sum up, we presented a flexible grating interferometer based only on two phase modulating gratings that eliminates the absorbing structures in the beam path. This allows high flux and ultimately dose efficiency that is critical for fast and dose sensitive experiments. The main strength of the system is its length scale tunability for dark-field imaging. This can be achieved easily by changing the distance between the two gratings that has no effect on the total system length and sample magnification. Such an option can be valuable for investigating porous samples or particle systems in a quantitative manner.

The authors would like to thank the technical and scientific staff from the Laboratory for Micro and Nanotechnology of PSI for their support. The patterning of the gratings was performed by EULITHA AG. Moreover, the authors would like to acknowledge the group of Professor Dr. Sander W. S. Gussekloo *et al.* of the Experimental Zoology Group, Wageningen University, Netherlands, for providing the seahorse sample and Gordan Mikuljan from PSI for his technical support. Part of this work has been supported by ERC Grant No. ERC-2012-StG 310005-PhaseX.

[1]T. Weitkamp, A. Diaz, C. David, F. Pfeiffer, M. Stampanoni, P. Cloetens, and E. Ziegler, Opt. Express **13**, 6296–6304 (2005).
[2]A. Momose, S. Kawamoto, I. Koyama, Y. Hamaishi, K. Takai, and Y. Suzuki, Jpn. J. Appl. Phys., Part 2 **42**, L866–L868 (2003).
[3]C. David, B. Nöhammer, H. H. Solak, and E. Ziegler, Appl. Phys. Lett. **81**, 3287 (2002).
[4]M. Stampanoni, Z. Wang, T. Thüring, C. David, E. Roessl, M. Trippel, R. A. Kubic-Huch, G. Singer, M. K. Kohl, and N. Hauser, Invest. Radiol. **46**, 801–806 (2011).
[5]D. Stutman, T. J. Beck, J. Carrino, and C. O. Bingham, Phys. Med. Biol. **56**, 5697–5720 (2011).
[6]T. Thüring, R. Guggenberger, H. Alkadhi, J. Hodler, M. Vich, Z. Wang, C. David, and M. Stampanoni, Skeletal Radiol. **42**(6), 827–835 (2013).
[7]V. Revol, I. Jerjen, C. Kottler, P. Schutz, R. Kaufmann, T. Luthi, U. Sennhauser, U. Straumann, and C. Urban, J. Appl. Phys. **110**, 044912 (2011).
[8]Z. Wang and M. Stampanoni, Phys. Med. Biol. **60**, 4123–4135 (2015).
[9]Z. Wang, N. Hauser, G. Singer, M. Trippel, R. Kubik-Huch, C. Schneider, and M. Stampanoni, Nat. Commun. **5**, 3797 (2014).
[10]M. Bech, A. Tapfer, A. Velroyen, A. Yaroshenko, B. Pauwels, J. Hostens, P. Bruyndonckx, A. Sasov, and F. Pfeiffer, Sci. Rep. **3**, 3209 (2013).
[11]S. Schleede, F. G. Meinel, M. Bech, J. Herzen, K. Achterhold, G. Potdevin, A. Malecki, S. Adam-Neumair, S. F. Thieme, F. Bamberg, K. Nikolaou, A. Bohla, A. Ö. Yildirim, R. Loewen, M. Gifford, R. Ruth, O. Eickelberg, M. Reiser, and F. Pfeiffer, PNAS **109**(44), 17880–17885 (2012).
[12]K. Hellbach, A. Yaroshenko, F. G. Meinel, A. Ö. Yildirim, T. M. Conlon, M. Bech, M. Mueller, A. Velroyen, M. Notohamiprodjo, F. Bamberg, S. Auweter, M. Reiser, O. Eickelberg, and F. Pfeiffer, Inv. Radiol. **50**(7), 430–435 (2015).
[13]F. Pfeiffer, M. Bech, O. Bunk, P. Kraft, E. F. Eikenberry, Ch. Brönnimann, C. Grünzweig, and C. David, Nat. Mater. **7**, 134–137 (2008).

[14]C. David, J. Bruder, T. Rohbeck, C. Grunzweig, C. Kottler, A. Diaz, O. Bunk, and F. Pfeiffer, Microelectron. Eng. **84**, 1172–1177 (2007).
[15]S. K. Lynch, V. Pai, J. Auxier, A. F. Stein, E. E. Bennett, C. K. Kemble, X. Xiao, W. Lee, N. Y. Morgan, and H. H. Wen, Appl. Opt. **50**(22), 4310–4319 (2011).
[16]W. Yashiro, Y. Terui, K. Kawabata, and A. Momose, Opt. Express **18**, 16890 (2010).
[17]F. Pfeiffer, T. Weitkamp, O. Bunk, and C. David, Nat. Phys. **2**, 258 (2006).
[18]S. Rutishauser, M. Bednarzik, I. Zanette, T. Weitkamp, M. Bšörner, J. Mohr, and C. David, Microelectron. Eng. **101**, 12–16 (2013).
[19]H. Miao, A. A. Gomella, K. J. Harmon, E. E. Bennett, N. Chedid, S. Znati, A. Panna, B. A. Foster, P. Bhandarkar, and H. Wen, Nat. Sci. Rep. **5**, 13581 (2015).
[20]H. Miao, A. Panna, A. A. Gomella, E. E. Bennett, S. Znati, L. Chen, and H. Wen, Nat. Phys. **12**, 830–834 (2016).
[21]M. Strobl, Sci. Rep. **4**, 7243 (2014).
[22]F. Prade, A. Yaroshenko, J. Herzen, and F. Pfeiffer, Europhys. Lett. **112**, 68002 (2015).
[23]S. Gkoumas, P. Villanueva-Perez, Z. Wang, L. Romano, M. Abis, and M. Stampanoni, Sci. Rep. **6**, 35259 (2016).
[24]B. J. Chang, R. Alferness, and E. N. Leith, Appl. Opt. **14**, 1592 (1975).
[25]E. E. Bennett, R. Kopace, A. F. Stein, and H. Wen, Med. Phys. **37**(11), 6047 (2010).
[26]The high tube voltage was chosen in order to increase the flux of the X-ray tube at the design energy. The higher energies generated are not detected by the X-ray detector since the efficiency is very low for high energies.
[27]P. Modregger, B. R. Pinzer, T. Thüring, S. Rutishauser, C. David, and M. Stampanoni, Opt. Express **19**, 18324 (2011).
[28]See http://www.cospheric.com for One-Stop Reliable Source of High Quality Microspheres.